Chapter 1

Development of iron oxide nanocubes-based nanocomposites for cancer cell sorting

…

1.1 Introduction

Cell sorting is defined as the isolation of cells from a heterogeneous biological sample. This powerful technique can find important applications in 1) the isolation of a desired population from a bulk mass of cells;[1] 2) the identification of unhealthy cells at the early stage of the disease;[2] 3) the detection of circulating cancer cells (CCCs) involved in tumor metastasis.[2] Magnetic sorting *via* the use of magnetic nanoparticles has been so far explored for several purposes, ranging from immunology for the isolation of immune system cells from organs and tissues, to cellular biology for the sorting of different cell types.[3-7] Nowadays, most of the tumors are recognized when their mass has reached a critical size and, often, when the metastatic process has already started.[8] The individuation of cancer cells or genetic materials from tumors at the initial stage of tumor growth would allow an early intervention, thus increasing the survival rate of the patients. A promising target is represented by circulating cancer cells (CCCs) or DNA derived by CCCs, which are involved in the spread of tumor inside the body.[2, 9-15]. Since biological materials circulate in the blood stream, they can be potentially recognized *via* a simple, fast and not invasive approach, by incubating magnetic materials (properly functionalized to recognize the target cells) on plasma sample, at a stage when biopsy cannot detects tumors. Despite of the powerful treatment methods already available, the early diagnosis of cancer in the patient is crucial for the prognosis.[16] The major limitation of using CCCs as diagnostic markers is related to their relatively low concentration in the blood, which makes difficult their individuation and isolation from other circulating cells.[17] Therefore, the development of tools able to recognize CCCs and their genetic side product in the blood stream is extremely important for an early stage cancer diagnosis and the application of an effective therapeutic procedure. Among the numerous types of cancer tumors, the ovarian cancer is the fifth leading cause of cancer-related death among women. Recurrence and poor prognosis are the major causes for a five year survival rate of about 45%.[18] Therefore, in this project it was developed a strategy to provide a fast and reliable detection and sorting of ovarian cancer cells for diagnosis. The proposed strategy includes the synthesis of magnetic nanobeads (MNBs), composed of magnetic nanoparticles, embedded in a polymeric shell that provides aqueous stabilization. The first work presented by *Di Corato et al.* relied on the use of spherical iron oxide nanoparticles for MNBs synthesis.[19] They demonstrated the efficient sorting and labeling of folate receptor positive cells. [19] Afterwards, the synthesis procedure was changed by *Materia et al.*[20] using iron oxide nanocubes with very high magnetic response.[21-23] These MNBs have a cumulative magnetic moment higher than that showed by magnetic nanobeads made with spherical nanoparticles. Thus, they have the peculiar properties to respond faster to an external magnetic field. Starting from these results the work here discussed aimed to obtain MNBs suitable for

labelling and enriching the cells/biological material of interest from a heterogeneous suspension. In order to sort the desired cells, targeting units on MNB surface are required. In particular, it must provide sensitivity and specificity to the nanocomposite toward the ovarian cancer cells. The biomolecule used in this project was the folic acid (FA), which is able to target folate receptor (FR). There are four different types of folate receptors. Three of them are expressed in adult cells while the fourth is related to the development of embryo. The three isoforms expressed in the adult are called FRα, FRβ and FRγ, and are responsible for the mediation of the extracellular folate uptake, essential carbon-donor for the synthesis of nucleic acid.[24] These receptors are expressed at very low levels in most tissues.[24] However, especially FRα is over-expressed in numerous cancers.[24] In particular, it is expressed in a variety of epithelial cancers and epithelial ovarian cancer (EOC).[25] Thus, FRα represents a promising target for the development of a targeting strategy of cancer cells, aiming to an early diagnosis of the disease. Several studies showed efficient conjugation of folic acid to different kinds of nanoparticle-based system.[26-30] Recently, *Wenting Liu et al.* demonstrated the efficacy of iron oxide nanoparticles functionalized with folic acid for the detection of ovarian cancer cells in the blood stream.[31] In addition, many works showed how the oriented ligation of biomolecules on the nanoparticles surface may improve the interaction with their target.[32-34] In the here presented work, a precise functionalization strategy was designed in order to provide biological activity, targeting efficiency and specificity to MNBs toward the desired cancer cells. In particular, a long PEG molecule was used to derivatize folic acid in order to expose it out of the nanocluster surface.[19, 31] The high mobility of folic acid anchored on a flexible molecule like PEG, may allow a more efficient interaction with folate receptor than if it is directly bound to the nanocluster surface *via* a rigid spacer, thanks to the increase number of possible orientations. The synthesized PEG-FA compound was than bound to the MNBs and used for cancer cells sorting. The system reported here was developed with the precise aim to sort ovarian cancer cells that circulate in the blood stream and those that grow inside the ascites of the peritoneal cavity, which are a prognostic marker of the ovarian cancer development.

1.2 Results and discussion

1.2.1 Targeting molecule: PEG-derivatized folic acid (PEG-FA) synthesis

In order to functionalize the MNBs with the folic acid (FA) as bioactive molecule, the first step was the synthesis of the FA functionalized with a poly(ethylene glycol) (PEG-FA). The attachment of PEG molecules on the surface would also increase the stability of the MNBs in solution by steric hindrance[35]. In detail, following a reported procedure,[36] folic acid was dissolved in DMSO and MES buffer (5:1 ratio) and reacted with 1-ethyl–3-(3-dimethylaminopropyl) carbodiimide (EDC) and *N*-hydroxysuccinimide (NHS), at 6 °C (ice bath) under nitrogen, in order to activate the carboxylic groups of FA molecules. After 1 h, α,ω-bis-aminopropyl-PEG (Mn = 1500 g/mol) was added and the temperature of the solution was gradually increased at room temperature (RT). The reaction mixture was subsequently allowed to stir for 12 h under nitrogen atmosphere (**Figure 1**). Then, the product was dialyzed against water to remove the free folic acid (see detailed procedure below).

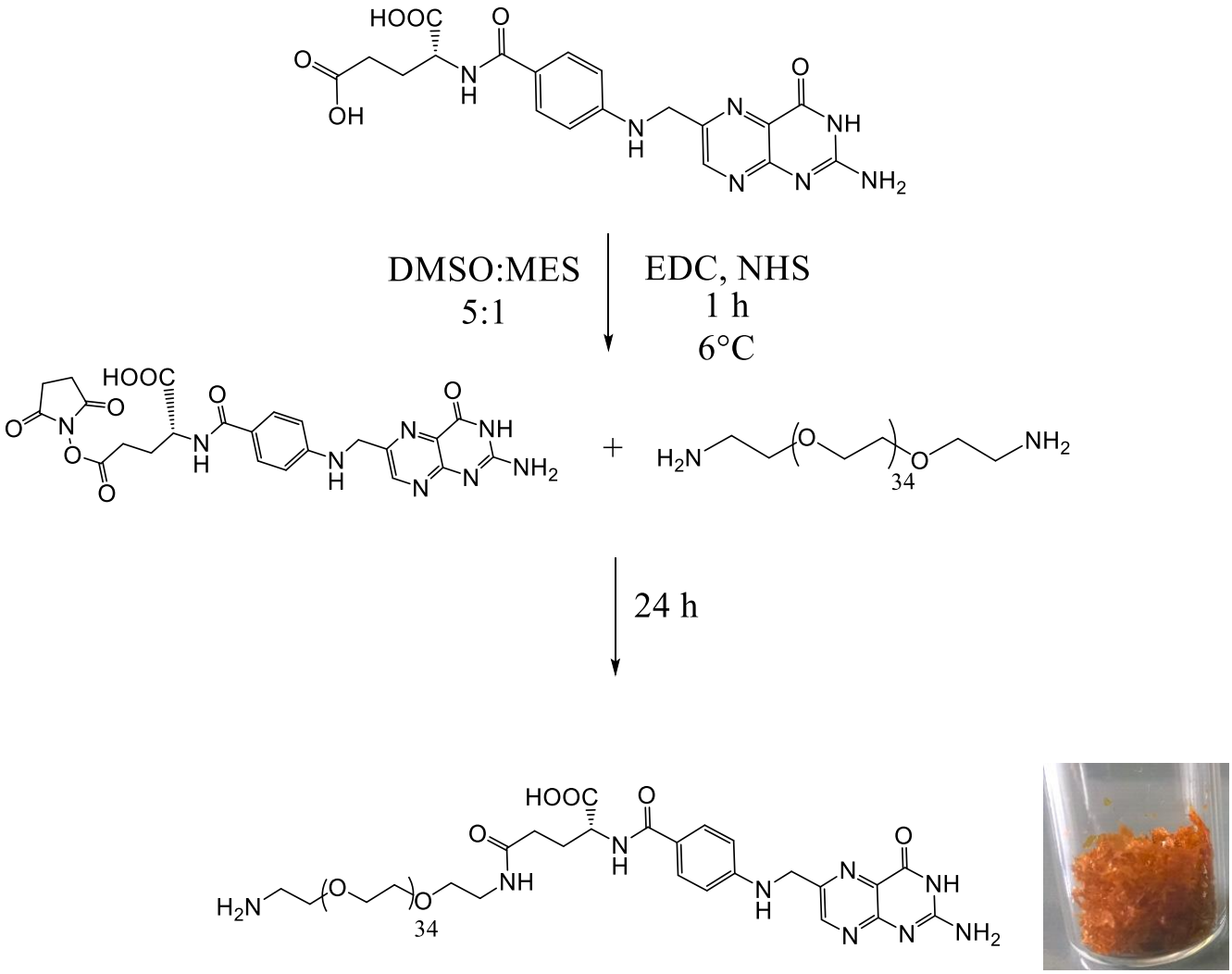

Figure 1. **Schematic representation of the NH_2-PEG-FA synthesis.** The picture on the right shows the obtained product after the reaction. The orange color indicates the presence of folic acid.

The final product was analyzed *via* ^{1}H-NMR spectroscopy in DMSO-d_6 (**Figure 2**). From the ratio of the integration of the characteristic FA signals and that of PEG backbone a degree of functionalization *f* of 74% could be estimated.

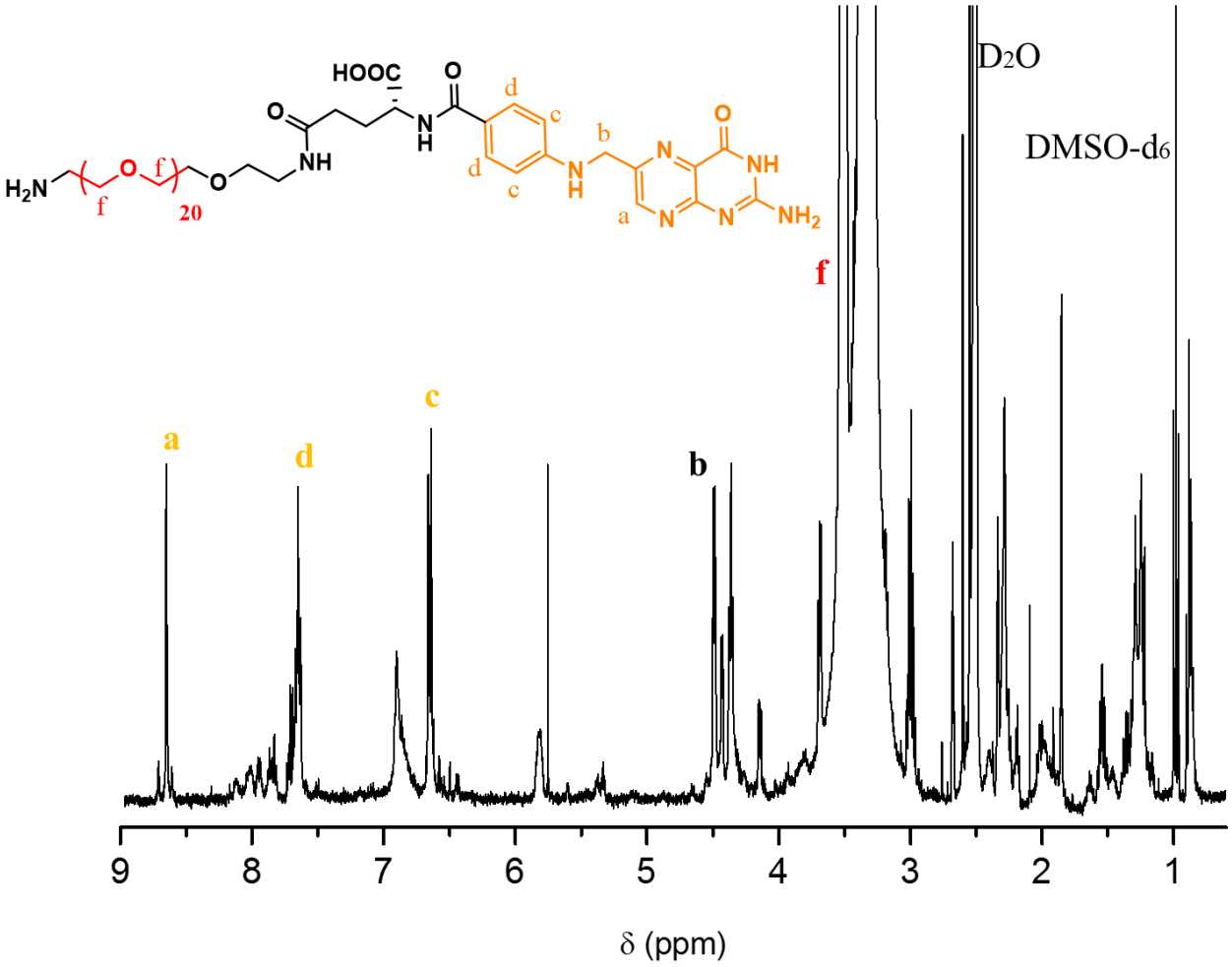

Figure 2. PEG-FA characterization. ^{1}H-NMR spectrum of NH_2-PEG-FA. δ_H(400 MHz, 128 scans, DMSO-d_6) 8.65 (1 H, **a**, fluor), 7.64 (2 H, **c**, fluor), 6.64 (2 H, **d**, fluor), 4.5 (2 H, **b**, fluor-CH), 3.54 (136 H, **f**, CH_2OCH_2).

1.2.2 Magnetic nanobeads synthesis

Magnetic nanobeads were synthesized according to a protocol set by *Di Corato et al.*[19], using spherical Fe_2O_3 NPs of 6 ± 2 nm and then adapted from *Materia et al.*[20] for iron oxide nanocubes. The functionalization step with PEG-FA required the knowledge of the amount of particles to be modified, in order to set the exact amount of reagents and molecules. However, for MNBs it was not possible to determine the amount of particles in solution or the concentration of polymer that enwrapped the NPs. In order to overcome this limitations, we assumed that the ratio polymer/NPs was constant in all the batches of MNBs and we considered just the concentration of Fe, *i.e.* the NPs concentration, in the nanobeads for calculating the amount of PEG to be used. Therefore, the Fe concentration was determined *via* ICP-AES (Inductively Coupled Plasma - Atomic Emission Spectroscopy). Since the Fe concentration was, with statistically good approximation, the same among different batches of MNBs, the amount of the reagents (EDC and PEG) was kept constant for all the functionalizations carried out (**Table 1**).

Table 1. Molar concentration of NPs per batch of nanobeads, determined via ICP-AES analysis. Each letter refers to each single reaction of the batches 1, 2 and 3.

Batch	C avg (μM)
1(A+B+C+D)	0.39±0.028
2(A+B+C+D+E+F)	0.353±0.01
3(A+B+C+D+E)	0.29±0.05
1+2+3	**0.34±0.05** (Err. 14%)

Several attempts were made for finding the best ratio of molecules of EDC and PEG per NPs (and then MNBs). The ratios of 78,000/125,000/400,000 molecules of EDC/NPs and 2,000/5,000/11,000 molecules of PEG/NPs were tested. Despite the different reagents' conditions adopted, soon after the reactions agglomeration and precipitation of the nanoclusters were observed. DLS analysis revealed a drastic increase of the size after the functionalization reaction (**Figure3a**), not explainable with the surface coverage of the PEG molecules. Moreover, the high polydispersity index indicated a non-homogeneous distribution of nanoclusters, also confirmed from the traces of aggregation in the size data weighed by volume and intensity (**Figure 3a**, inset). Furthermore, TEM pictures (**Figure 3b** and **3c**) revealed the presence of unfolded polymer around nanobeads (black arrows in **Figure 3b** and dotted line in **Figure 3c**). We conclude that the binding of EDC first and PEG later was able to miss fold and unroll the outer polymeric shell of nanobeads. This effect compromised the stability of nanobeads and explained the increase in DLS diameters.

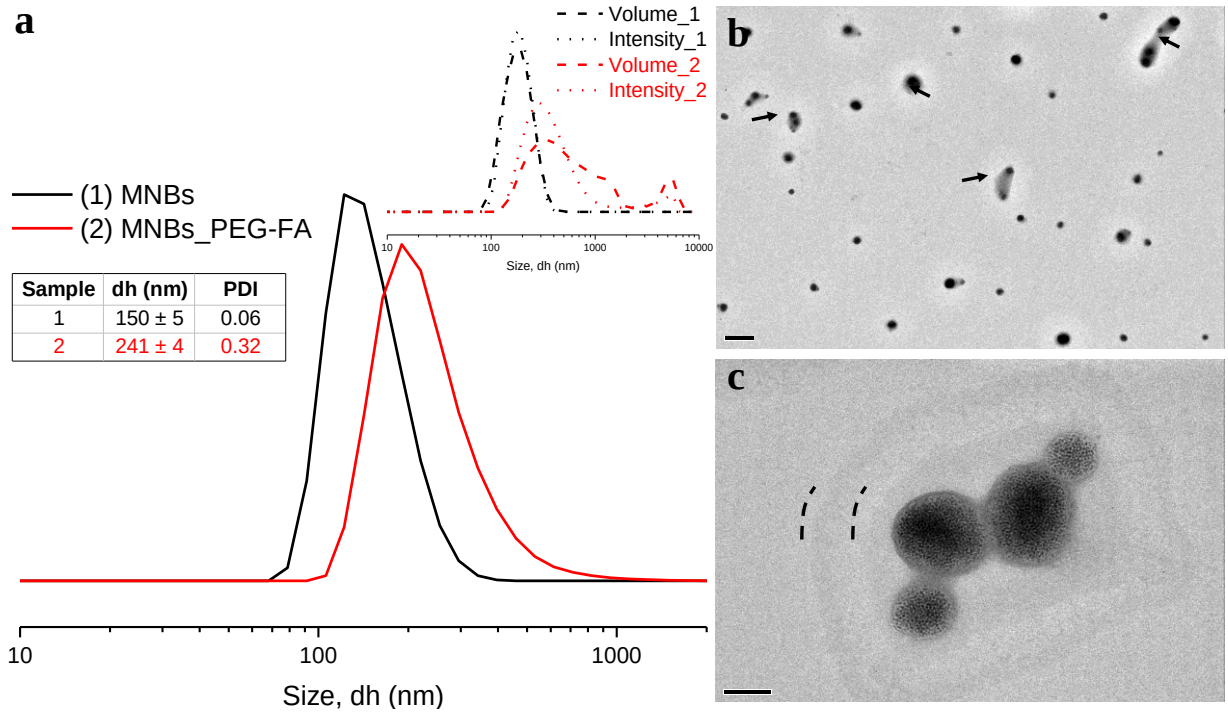

Figure 3. MNBs characterization of MNBs after functionalization. **a)** DLS graph shows the size weighed by number of the nanobeads obtained. Table in the inset reports the hydrodynamic diameter (dh) and polydispersity index (PDI). In the inset, DLS graph shows the size weighed by volume and intensity for MNBs (black dotted and dashed lines) and MNBs_PEG-FA (red dotted and dashed lines). **b)** TEM picture shows the presence of unfolded

polymer around nanobeads (black arrows). Scale bar 0.5 µm. **c)** TEM picture magnification shows a thick polymer layer around each single nanobeads (black dotted lines). Scale bar 100 nm.

Consequently, for the successful surface functionalization of the beads, a modification to the standard MNBs synthesis procedure was required. A modified version of the poly(maleic anhydride-*alt*-1-octadecene) (in the following called PIII) was synthesized by reacting the poly(maleic anhydride-*alt*-1-octadecene) with 2,2'-Ethylenedioxy-*bis*-ethylamine (EDBE), at a ratio of 1 to 20, which corresponds to a 10% of the anhydride reacted with the EDBE groups. The EDBE molecule is able to crosslink the polymer chains on the beads by the reaction of its amine groups with the anhydride rings of the polymer. The EDBE reaction with polymer was performed in tetrahydrofuran (THF), a solvent in which both compounds are well soluble.[37] The reaction was let to proceed for 12 h at 65 °C in a sealed vial, under shaking. The change of the solubility in chloroform for the functionalized polymer indicated that the reaction took place (**Figure 5b**). Indeed, while the poly(maleic anhydride-alt-1-octadecene) is very soluble in that organic solvent, the turbidity of the solution of the EDBE-modified polymer indicated it's spare solubility in chloroform (**Figure 5b**). This is consistent with the increase of hydrophilicity of the polymer upon the attachment of a polar molecule like EDBE. Moreover, it was decided to move toward the synthesis of MNBs made up with nanocubes (NCs), due to the better magnetic properties of this kind of nanoparticles compared to the spherical ones, as clearly highlighted in chapter 1. Fe_2O_3 nanocubes of 15 ± 3 nm were used. The procedure followed was based on the protocol set by our group[20], with some modifications. The modified polymer was mixed with the NCs in THF and shaken for ca. 30 s Afterwards, water (instead of acetonitrile as in the standard procedure) was added to the mixture using a syringe pump to induce the NCs and polymer interaction and consequently the beads formation. After the synthesis, the remaining THF was let to evaporate slowly and the MNBs were filtered (PVDF 0.45 µm filter). Noteworthy, the yield after filtration was in the range of 75%-85% (referred to the iron amount). Thus, with this modified procedure, nanobeads soluble in aqueous media were directly obtained (**Figure 4a**). The detailed procedure for MNBs synthesis is reported in "materials and methods" section. DLS, TEM and HR-MAS NMR (High Resolution Magic Angle Spinning NMR) characterized the obtained nanobeads (**Figure 4, 5** and **6**). The DLS graph in **Figure 4b** shows that MNBs have a monomial size distribution and a high stability, as no aggregates were present. Moreover, zeta potential measurements showed a strong negative surface charge of -40 ± 3 mV, which contributed to their stabilization in aqueous media (**Figure 4b**, table in the inset).

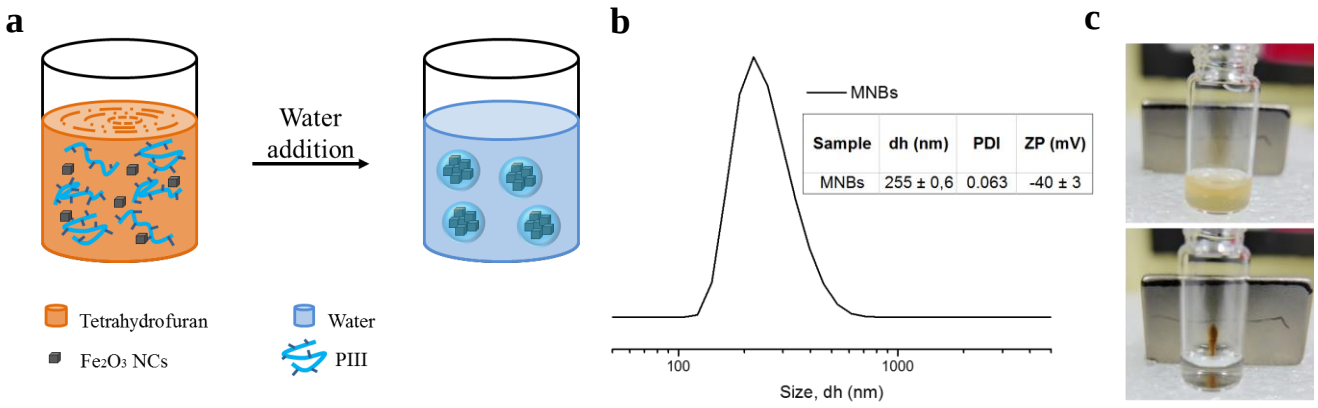

Figure 4. **MNBs characterization and magnetic response. a)** Scheme of the procedure developed for the synthesis of nanoclusters made with nanocubes **b)** DLS graph shows the weighed number of the nanobeads

obtained with iron oxide nanocubes. Table in the inset reports the obtained hydrodynamic diameter (dh), polydispersity index (PDI) and zeta-potential (ZP). **b)** By applying an external magnetic field (0.4 T) generated by a NdFeB magnet, it was possible to easily and quickly collect the MNBs.

High resolution-magic angle spinning NMR (HR-MAS NMR) analysis was carried out in water containing 10% D_2O. In contrast to the standard NMR technique, HR-MAS allow the NMR analysis of magnetic nanoparticles. The measurement revealed the presence of the crosslinker among the polymeric chains. Indeed, the peak (a) (ppm: δ: 3.6) in **Figure 5a** can be attributed to the presence of the ethylene glycol unit of EDBE, which is indeed absent in the same region of the spectrum form the non-functionalized polymer (b). In addition, the peak (c) (ppm: δ: 1.2), related to the carboxylic group derived from the opening of the maleic anhydride, decreases in intensity after the binding of EDBE. The other peaks in between can be attributed to the groups of the polymer.

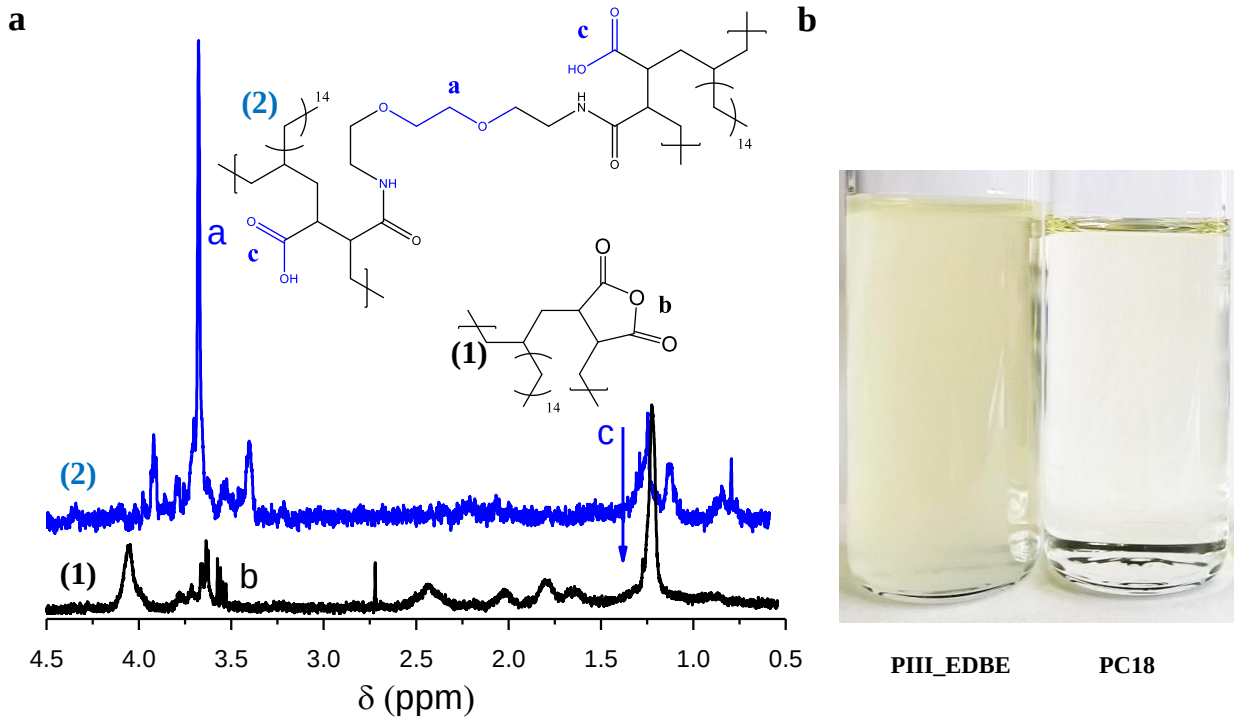

Figure 5. **Characterization of PIII_MNBs**. **a**) HR-MAS NMR spectra of MNBs, synthetized with PIII polymer (chemical structure in the graph, 2) (a). (400 MHz, water-d_2 10%, δ: 3.6 (4H, **a**, CH_2OCH_2), 1.2 (1 H, **c**, CHCO)). **b)** Pictures of the initial solution of poly(maleic anhydride-*alt*-1-octadecene) known as PC18 (right) and of the polymer after the functionalization with EDBE molecules (PIII_EDEB, left), in chloroform.

Transmission Electron Microscopy (TEM) images (**Figure 6**) show a homogeneous population of beads with a spherical shape and a diameter of ca. 200 nm, containing iron oxide nanocubes clearly encapsulated by polymeric shell.

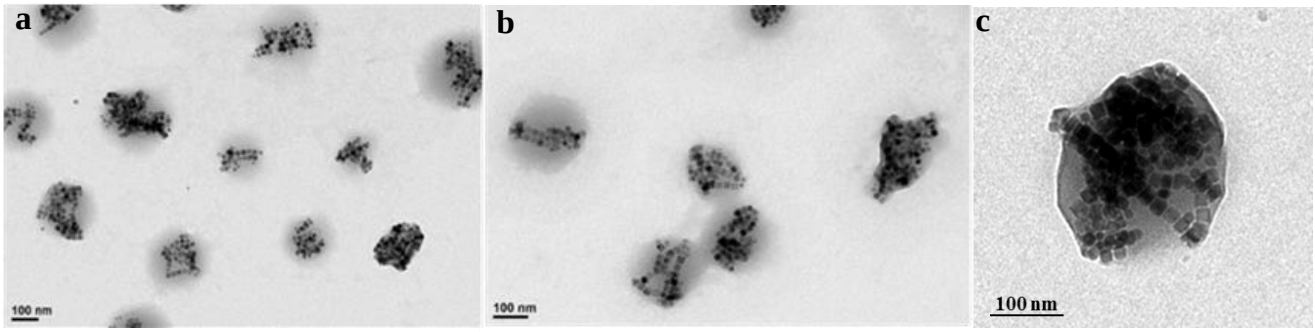

Figure 6. TEM micrographs of MNBs. a) and **b)** MNBs made up with nanocubes. **c)** Magnification of a single nanobead.

1.2.3 Functionalization of magnetic nanobeads with PEG-FA

The application of the cross-linked polymer for the preparation of the nanobeads resulted in a much more stable polymeric shell, which was not affected by further functionalization steps, avoiding miss folding events of the polymer. In order to bind PEG-FA to MNBs, a modified procedure set by our group was applied.[19] MNBs were incubated with EDC for 10 min in a 1:3 mixture of water and borate buffer. Then, NH_2-PEG-FA (MW ca. 2000 g/mol) was added and the mixture was allowed to stir for 4 h at room temperature (RT). The nanobeads were subsequently cleaned from the excess of the reagents (EDC and PEG-folic acid) using magnetic separation (**Figure 7a**). The purity of the nanocubes was confirmed by spectrophotometric analysis. Indeed, the excess of EDC and folic acid (peaks at 225[38] and 267[39] nm, respectively), was completely removed after the third washing step and no trace of free reagents was detected in the supernatant (**Figure 7b)**.

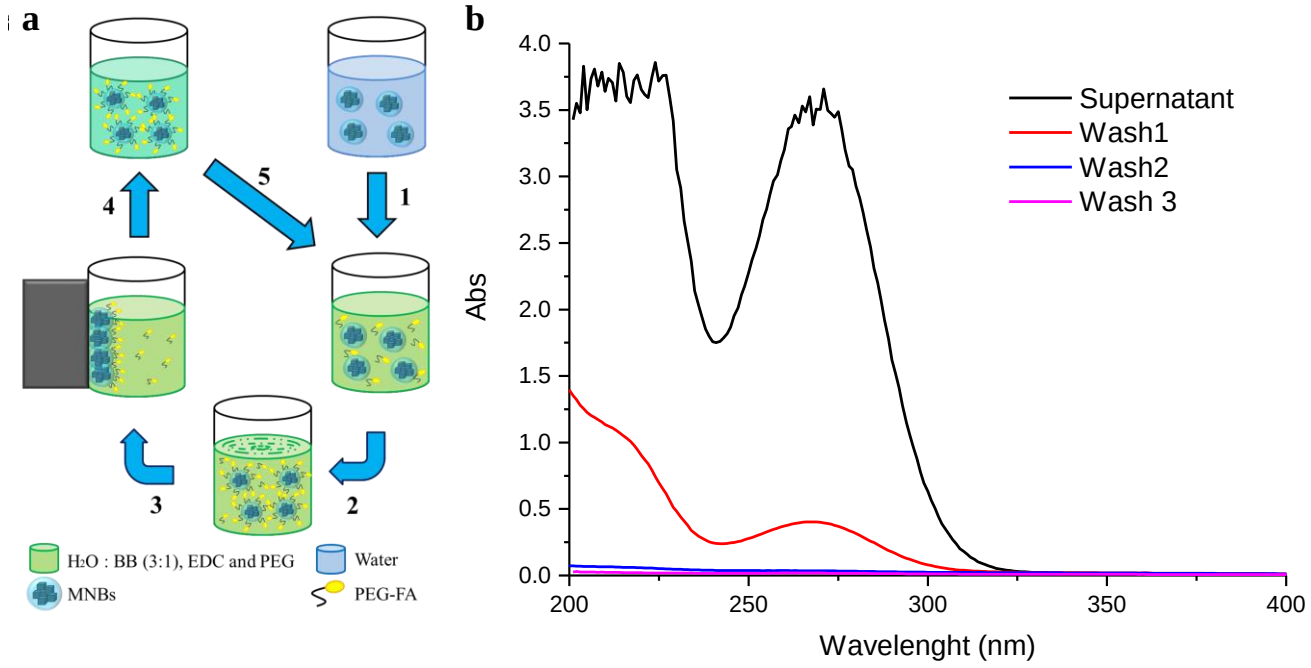

Figure 7.**Cleaning of PEGylated MNBs**. **a)** Schematic representation of the cleaning step following the MNBs functionalization. (**1**) The addition of EDC and PEG, in a mixture of water and borate buffer (BB), was followed

by 4 h of mixing under stirring (**2**). In order to remove the excess of the reagents, MNBs were collected in 5 minutes to a magnet (**3**) and re-dissolved in fresh water : BB mixture (**4**). The cleaning process was repeated three times **(5)**. **b)** Absorbance spectra of the supernatants of MNBs reacted with PEG-FA. After three washes the signals from EDC at 225 nm and folic acid 267 nm disappeared. The three washes are indicated with the letter W and the corresponding number.

The products of the conjugation were characterized by DLS and pH titration. As a control, MNBs PEGylated with the bis(amine)PEG were used (namely MNBs-PEG). DLS results in **Figure 8a**, show a significant increase of the beads size after PEGylation. Nevertheless, no significant variation in the size of the beads functionalized with PEG (green line) and PEG-FA (olive line) was observed, reasonably due to the low size difference between the two molecules. Noteworthy, after the PEG addition, MNBs appeared stable and monodisperse, with no traces of aggregation.

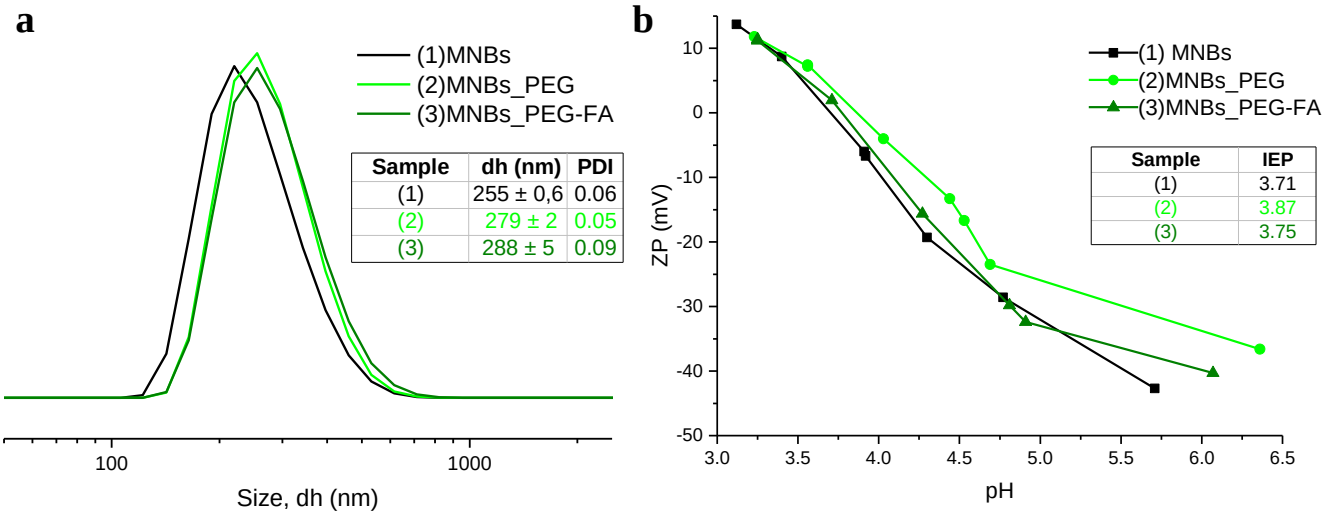

Figure 8. **Characterization of functionalized MNBs**. **a)** DLS graph shows the weighed number of pristine beads (black line), PEGylated beads (green line) and beads functionalized with PEG-FA (olive line). The table shows the corresponding size and PDI values. **b)** pH titration graphs of beads. Black line: MNBs. Green line: MNBs_PEG. Olive line: MNBs_PEG-FA. The table shows the corresponding IEP values.

Titration experiments were carried out on both samples (MNBs-PEG and MNBs_PEG-FA) in order to investigate the change of the surface charge at different pH values and to obtain the correlated isoelectric points (IEPs) which could confirm the functionalization of the beads surface. As shown in **Figure 8b**, the titration curves change significantly for the different samples, as well as their IEP. Indeed, MNBs (black line) showed at pH = 6 a more negative ZP values compared to the other samples, for the higher content of carboxylic groups on their surface. Moreover, the pristine beads reached the IEP at lower pH, consistently with the higher concentration of H^+ needed for saturating the carboxylic groups. Interestingly, MNBs functionalized with PEG-FA (olive line) had an IEP close to that of MNBs and considerably lower than that of MNBs_PEG (green line). This was explainable with the presence of a carboxylic group in the folic acid, which decreased the ZP value compared to PEG-amine.

1.2.4 Stability proofs of magnetic nanobeads functionalized with PEG-FA

The stability of the obtained MNBs was monitored in the presence of fetal bovine serum (FBS). FBS is added to almost all of the culture media used for *in vitro* cellular experiments and could induce precipitation or aggregation of nanoparticles, due to its high protein content. More specifically, these proteins tend to adsorb on the surface of the nanomaterials forming the so-called protein corona.[40-42] This phenomenon can be benefic to stabilize the NPs in solution if induced in a controlled manner.[43, 44] On the other hand, a thick protein corona might saturate the surface of the nanoobjects and can seriously compromise the solubility of the latter in biological media,[45, 46] as well as their biological activity.[47] To prove that MNBs retained their stability in biological media upon PEGylation,[35] MNBs-PEG-FA were incubated in PBS (0.1 M, pH=7.4) supplemented or not with FBS 10%, at 37 °C, in order to evaluate the effect of the protein on their stability (**Figure 9**). As control, the stability of plain MNBs was also tested. DLS of both samples was performed upon incubation overtime. Despite a comparable stability in PBS (**Figure 9a**), the hydrodynamic diameters of MNBs in the presence of FBS is significantly higher than that of MNBs_PEG-FA already after 5 minutes of incubation, indicating the higher protein absorption (**Figure 9b**). In the following 30 minutes, MNBs size increased drastically when compared to PEGylated sample (MNBs_PEG-FA). After 3 h of incubation, MNBs formed large aggregates and precipitated after 48 h. MNBs_PEG-FA retained their stability up to 48 h, as shown by their stable hydrodynamic diameter. This indicates a much higher stability of the PEGylated nanobeads in FBS media than that of pristine synthesized MNBs as it is known that PEG reduces protein absorption.[35]

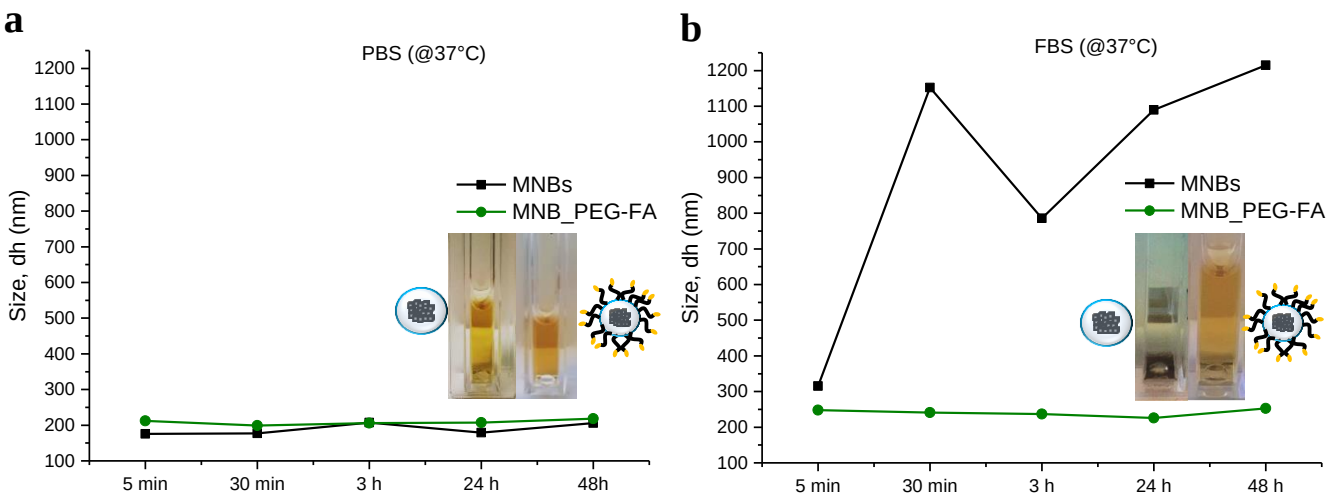

Figure 9. **Stability proofs of MNBs**. DLS Size values of magnetic nanobeads plotted against the incubation time in **a)** PBS and **b)** FBS 10%. In black is shown the size distribution profile for MNBs, in red for PEGylated MNBs.

1.2.5 Magnetic cell separation using functionalized magnetic nanobeads

MNBs_PEG-FA were then tested for their ability to specifically bind cells overexpressing folate receptor (FR; cells referred as FR+). The tumorigenic KB line (subline of the ubiquitous KERATIN-forming tumor cell line HeLa) was selected as the cell model for sorting studies. Such experiments had the aim to provide important information on the suitability of MNBs for being used for magnetic cell sorting. [19] Before starting the experiments with cells, the MNBs were washed twice with PBS 0.1 M, pH=7.4. Then,

KB cells were incubated at 4 °C with nanobeads functionalized with PEG-NH_2 or PEG-FA, varying the incubation time from 15 min to 1 h and keeping a ratio of 1 μg of iron/100,000 cells and 1 μg of iron/50,000 cells. Once recovered, the cells were centrifuged and washed in order to remove the MNBs in excess. Subsequently, the cells were flowed through MACS column (Miltenyi Biotech), which is able to retain just the magnetically labeled cells. How this column works was previously shown in the introduction, at paragraph 4. **Figure 10** shows the binding percentage of the MNBs_PEG-FA (dark green bar) and MNBs_PEG (light green bar) incubated at 4 °C with KB cells, for 15 minutes, 30 minutes and 1 h. The results in **Figure 10a** show a significant binding difference between the MNBs_PEG-FA (43% after 60 minutes) and MNBs_PEG MNBs (5% after 60 minutes). However, the overall binding value was low even for the MNBs_PEG-FA. Thus, it was decided to increase the ratio μg iron per number of cells during the incubation to 1:50000 (**Figure 10b**). The binding of MNBs_PEG-FA increased, reaching a percentage of 81% after 60 minutes, while the unpecific binding of MNBs_PEG remained low (11% after 60 minutes). In this case, even after 30 minutes of incubation MNBs_PEG-FA showed interesting sorting ability (70.5%) without compromising their specificity (unspecific binding equal to 5.5%). Noteworthy, no binding retention inside the magnetic column was observed for non-magnetically doped cells (control).

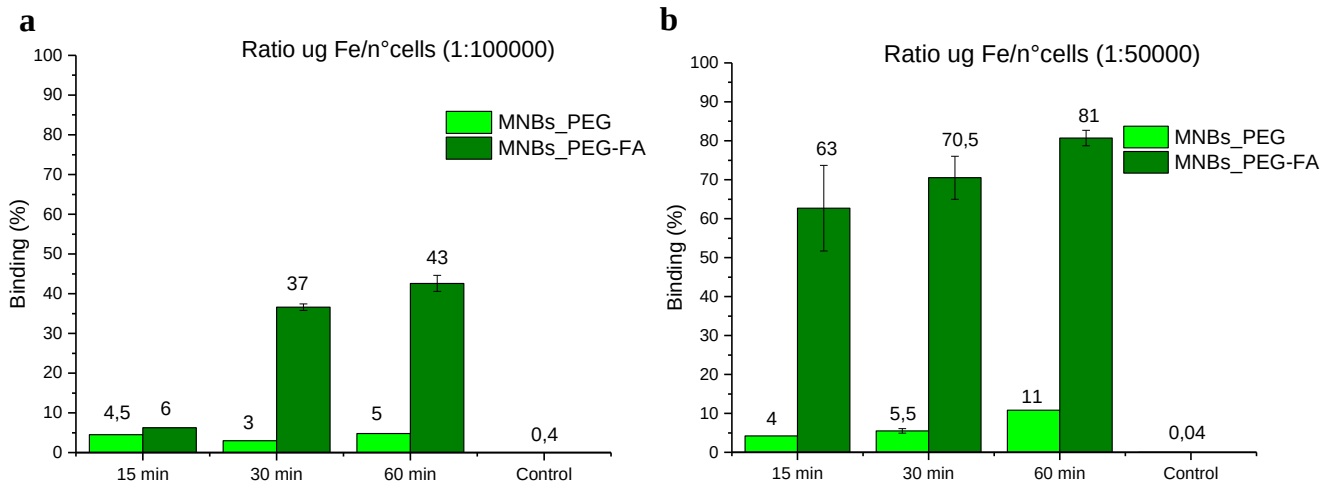

Figure 10. Sorting efficiency of MNBs. The histogram shows the binding percentage of MNBs and MNBs_PEG-FA to the KB cells at **a)** 1 μg of iron/100,000 cells ratio and **b)** 1 μg of iron/50,000 cells ratio. The control refers to the KB cells flowed through the column without MNBs.

The preliminary results obtained in the ovarian cancer cell sorting, demonstrated the specificity of the MNBs_PEG-FAfor its cell target. Folic acid provided specificity to the MNBs. Moreover, MNBs were efficient in separating the magnetically labeled cells.

1.2.6 Uptake studies and cell-iron content

In order to confirm that the sorting was determined by the binding of the magnetic nanobeads, the amount of iron found inside the cells was determined *via* ICP-AES. **Figure 11a** shows the pellet of the cells incubated with MNBs_PEG (dashed light green square) and MNBs_PEG-FA (dashed dark green square) and after the washing from the excess of MNBs. It is clearly visible the presence of the MNBs bound to

the cells in case of MNBs_PEG-FA (dashed dark green square), as indicated by the brownish color of the pellet. Whereas the pellet of the cell incubated with MNBs_PEG is white, indicating a low amount of MNBs. Further experiments carried out using the best condition found for sorting (1 μg of iron/50,000 cells) demonstrated the good reproducibility of the system developed (**Figure 11b**). The fact that the sorting efficiency (S_e) was driven effectively by the MNBs had confirmation from elemental analysis. The iron content obtained via ICP was normalized for the total cell number. In case of MNBs_PEG-FA the iron content inside the cell fraction was more than three times higher than those collected in case of MNBs_PEG (**Figure 11c**). Moreover the amount of Fe collected with the cells was just half of the total amount employed in the sorting experiment (**Figure 11d**), indicating that a good separation efficiency could be reached with a lower amount of magnetic material.

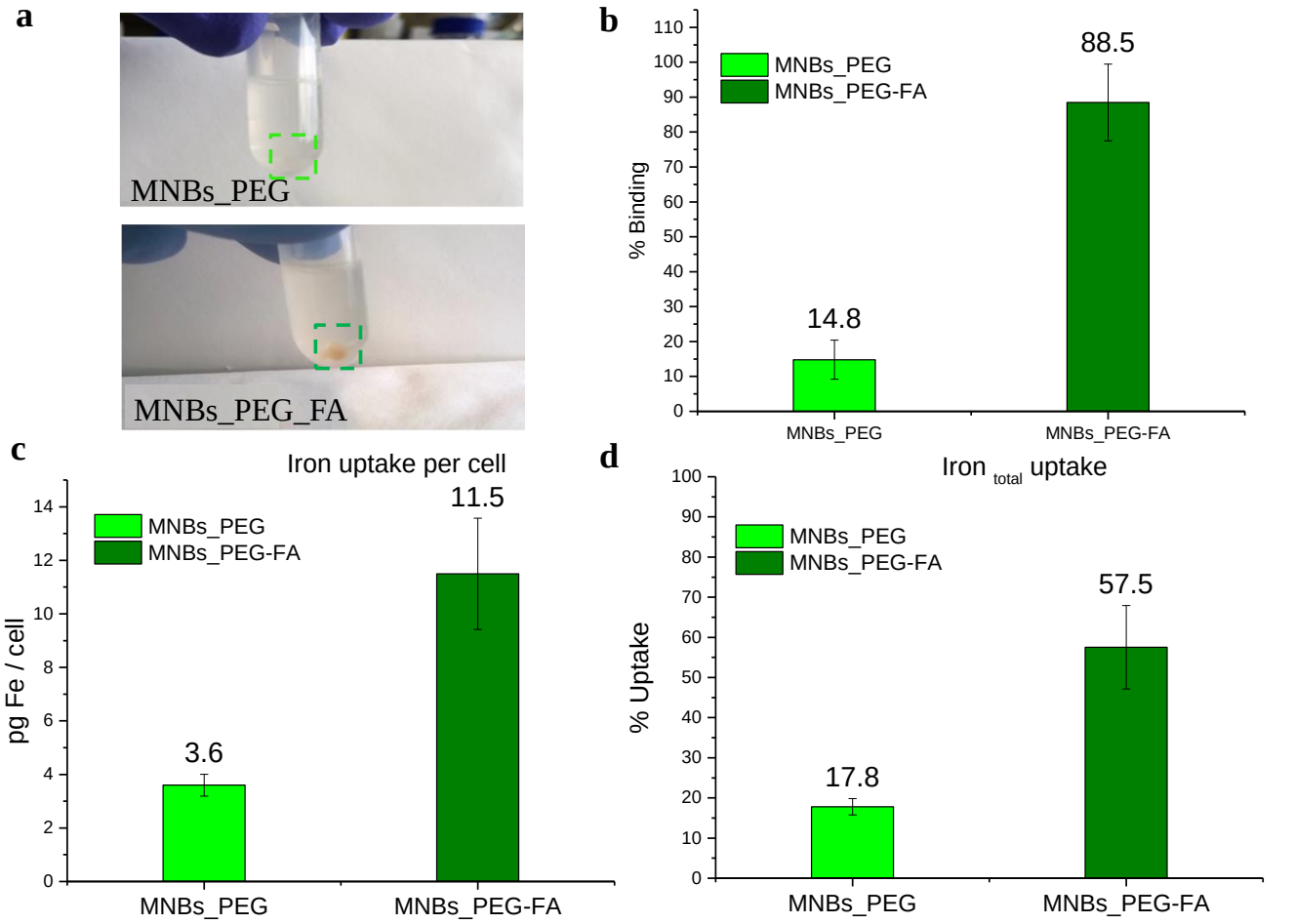

Figure 11. **Characterization of the sorting properties of MNBs. a)** Pictures of the cell pellets after the incubation with MNBs_PEG (top and dashed light green square) and MNBs_PEG-FA (bottom, dashed dark green square). **b)** S_e of the MNBs for KB cells. **c)** Nanoclusters uptake by KB cells (FR+) express as pg of iron per cell and **d)** uptake percentage, relative to the total amount of iron used for the incubation. MNBs_PEG indicates the sample PEGylated with the non- derivatized PEG, while MNBs_PEG-FA indicates the sample functionalized with FA.

1.3 Conclusion and perspectives

A new method for the synthesis of magnetic nanoclusters was developed. The standard procedure reported in literature for the synthesis of the magnetic nanobeads [19, 20] showed some issues regarding the colloidal stability of the nanoclusters upon conjugation with small PEG-modified folic molecules. Indeed, it was hypothesized that the poor interaction of polymer alkyl chains with the nanoparticles surfactants, which involves the outer layer of the polymeric shell, determined the instability of the nanobeads following the attachment of long PEG molecules on their surface. This instability was attributed to miss folding of the polymer that not only affect the overall colloidal stability of the nanocomposites but also the functions of the attached molecules. Thus, in order to overcome this problem, the polymer poly(maleic anhydride-*alt*-1-octadecene) shell was bridged, by introducing a diamine EDBE as crosslinker. Due to its small length, the rational beyond the use of this molecule was the creation of a branched polymeric structure able to increase the strength and stability of the polymer shell on the nanobeads. Noteworthy, due to the increased hydrophilic nature of the polymer, the nanobeads synthesis was also improved by replacing, as precipitating solvent, acetonitrile with water and thus reducing the use of organic solvent for MNBs production. The PEGylation with the biological relevant molecule PEG-FA was demonstrated to provide stability to the MNBs in complex biological media and to make the nanoclusters able to interact with cells overexpressing the folate receptor. Thanks to these features, the MNBs developed were successfully employed for magnetic sorting application. The promising results obtained with the isolation of positive cells for the overexpression of folate receptor open the way for a deeper investigation of MNBs sorting ability. Further experiments will be performed for the sorting of ovarian cancer cells in the ascitic liquid withdrawn from the peritoneal cavity of patients, aiming to accomplish an efficient diagnosis of the cancer at early stages of development. However, the lack of specificity of folic acid for the different folate receptor species has to be considered. Indeed, MNBs functionalized with PEG-folic acid may also bind to macrophages present in the ascitic fluid, which express folate receptor β.[25] This would impair the sorting efficiency of ovarian cancer cells. This limitation can be solved by using antibody or antibody fragments specific for folate receptor α and thus for ovarian cancer cells. Future experiments will help to clarify this issue.

1.4 Materials and methods

Nanocubes synthesis

Iron oxide (Fe_2O_3) nanocubes (NCs), with an edge size of 15 ± 3 nm were synthetized according to a procedure previously set in our group.[48] Briefly, in a 50 mL three neck flask, 0.353 g (1 mmol) of iron(III) acetylacetonate, 0.69 g (4 mmol) of decanoic acid and 2 mL of dibenzyl ether (DBE) were dissolved in 23 mL squalane. After degassing for 120 min at 65 °C, the mixture was heated up to 200 °C (heating ramp was 3 °C min^{-1}) and kept at this temperature for 2.5 h (a shorter "aging time" at 200 °C led to lower reproducibility as well as to broadening of the size and shape distributions of the final particles). The temperature was then increased at a heating rate of 7 °C min^{-1} to 310 °C or reflux temperature and maintained for 1 h. After cooling down to room temperature, 60 mL of acetone were added and the solution was centrifuged at 8500 rpm. The supernatant was then discarded and the black precipitate was dispersed in 2–3 mL of chloroform: this washing procedure was repeated at least two more times. Finally, the collected particles were dispersed in 15 mL of chloroform. The concentration of the final nanocubes was determined by ICP analysis.

Synthesis of PEG-FA

Folic acid (58 mg; 0.13 mmol) was dissolved in DMSO and reacted with 1-ethyl–3-(3-dimethylaminopropyl) carbodiimide (EDC, 1.3 mmol; 10 eq.) and N-hydroxysuccinimide (NHS, 1.3 mmol; 10 eq.), in ice bath at 6 °C, in order to activate the carboxylic groups of FA molecules. After 10 minutes, O,O'-Bis(3-aminopropyl)polyethylene glycol (Mn = 1500 g/mol; 200 mg; 0.13 mmol) was added and the solution was allowed to stir for 12 h. Then, the product was dialyzed against water using a RC- membrane (cut-off 1000 g/mol). The excess of unreacted folic acid precipitated due to its poorly solubility in pure water (1.6 mg/mL at 0 °C).[49] Using a 0.2 μm PVDF filter it was removed from the PEG product. The final product was freeze-dried and analyzed via ^{1}H-NMR spectroscopy. ^{1}H NMR spectra were recorded on a Bruker AV-400 NMR spectrometer (Rheinstetten, Germany) operating at 400 MHz (64 scans) in deuterated dimethyl sulfoxide (DMSO-d_6) ppm: δ: 8.65 (**a**), 7.64 (**c**), 6.64 (**d**), 4.5 (**b**), 3.68 (**e**), 3.51 (**f**).

Synthesis of PIII polymer

The EDBE addition polymer reaction was performed in tetrahydrofuran (THF). 1 mmol of poly(malic anhydride-*alt*-1-octadecene) (PC18) was dissolved in 10 mL of THF and the temperature of the solution increased at 65 °C. Afterwards, 0.05 mmol (1:20 ratio) of 2,2'-Ethylenedioxy-*bis*-ethylamine (EDBE) were added and the mixture was let to react for 12 h at 65 °C. The product was then cooled down at room temperature, filtered using a PTFE 0.2 μm filter, and dissolved in 20 mL of THF at the final concentration of 50 mM.

Synthesis of MNBs

According to the new procedure set, 300 μL of PIII (50 mM in THF) were transferred in a 40 mL vial and the solvent evaporated using a nitrogen flow. Then, 170 μL of nanocubes (15 ± 3 nm, Fe_2O_3, 1.7 g/L Fe, in $CHCl_3$) were mixed with the polymer and the solvent evaporated. Subsequently, 2 mL of THF were added to the mixture under sonication at 40 °C, with the vial sealed, for 1 minutes. Afterwards, the reaction mixture was shaken at 1700 rpm. After 30 sec, 17 mL of water were added (16 mL/minute),

promoting the formation of the nanobeads. After the reaction, the remaining THF was let to evaporate under gentle shaking for 12 h. The final MNBs were filtered using a PVDF filter (0.45 µm) and collected. The yield of the filtered nanobeads was calculated as 75%-85%, considering the amount of iron before and after the filtration step.

HR-MAS NMR

Each magnetic nanobeads sample was washed three times in D_2O solution. The samples were inserted into a zirconium oxide 4 mm outer diameter rotor with an additional drop of D_2O to provide a field-frequency lock for the NMR spectrometer. An insert was placed into the rotor to make a spherical sample volume of 25 µL. A cap was finally added as a closure of the rotor and the assembled device was used immediately for NMR analysis. All samples were randomized during analysis to reduce any potential systematic errors. All ^1H NMR spectra were recorded on a Bruker AV-400 NMR spectrometer (Rheinstetten, Germany) operating at 400 MHz for ^1H, equipped with a high-resolution magic angle spinning probe at a spin rate of 5000 Hz. Sample temperature was regulated using cooled N_2 gas at 283 K during the acquisition of spectra to minimize spectral degradation. ppm: δ: 3.595 (b), 3.675 (a), 1.175 (c).

UV/Vis analysis

UV/vis absorption spectra of the supernatant and washes collected after the functionalization raction were recorded on a Cary 50 UV/vis/NIR photospectrometer using PMMA disposable cuvette of 1 cm optical path length.

MNBs characterization via dynamic light scattering analysis (DLS)

Hydrodynamic size distribution and zeta potential were measured using a Malvern Zetasizer operated in the 173° backscattered mode on highly diluted aqueous solution of MNBs. The measurements were performed at 20 °C. Dynamic light scattering analysis (DLS) calculates the hydrodynamic diameter (dh) of particles in colloidal solution, giving information about homogeneity and stability of the nanoparticles in suspension. Moreover, the software of the instrument also provides a polydispersity index (PDI), which furnishes indication of the solution monodispersity. Lower is the PDI value, higher the homogeneity of the solution. Consequently, lower is the tendency to aggregation of the nanoparticle sample. In addition to the hydrodynamic size, the same instrument can also perform the zeta potential (ZP) measurements related to the surface charge of nanoparticles. This kind of analysis can give important information about the nanoparticles' surface properties such as the presence of charged groups from specific functionalizations as well as it can be used to infer about their stability in different solutions.

Low-resolution Transmission electron microscopy (TEM)

Low-resolution TEM micrographs were taken using a JEOL JEM-1011 microscope operated at 100 kV. The samples were prepared by drying a drop of diluted particle suspensions on 400 mesh ultra-thin carbon coated TEM copper grids. The particle size distribution was analyzed using the automatic particle size analysis routine of ImageJ software on a low magnified TEM micrograph.

Functionalization of MNBs with PEG-FA

MNBs (0.1 μM), dissolved in 500 μL of a 1:3 mixture of borate buffer (pH=9) and water, were incubated for 10 min with 40 mM of EDC (400,000 molecules per iron nanoparticle). Then, 1.1 mM of amine-PEG-FA (Mn= 2000 g/mol) (11,000 molecules per iron nanoparticle) was added and the mixture was let to react for 4 h under stirring. Nanobeads were subsequently cleaned from the excess of the reagents five times in borate buffer, using a permanent NdFeB magnet generating a magnetic field of 0.4 T.

Cell sorting and counting

$5x10^5$ KB cells were incubated at 4 °C with 5 or 10 μg (referred to the iron content) of nanobeads, keeping a ratio of 1 μg/100,000 cells and 1 μg/50,000 cells respectively. The incubation times varied from 15 minutes to 1 h. After the incubation, the cells were centrifuged at 4 °C for 5 minutes at 1000 rpm in order to remove the excess of beads, which remained in the supernatant, from the suspension. The cells were then resuspended in 500 μL of PBS and eluted into a Magnetic Cell Sorting MACS® MS column (Milteny Biotech) for magnetic sorting. An excluded volume, three washes and a collected fraction were recovered. The cells were counted using NucleoCounter® NC-100™ (ChemoMetec). The same volume of cells, Reagent A100 (lysis buffer) and Reagent B (stabilizing buffer) were added to the test tube for the total cell count (cells/mL). The sorting efficiency (S_e) was calculated as percentage of the amount of the collected cells compared to the total amount of cells initially incubated with the nanocubes, according to the following equation:

$$S_e = \frac{500{,}000-(CC)}{500{,}000} \text{ x } 100 \qquad (1)$$

ICP-AES analysis of Fe

Cells samples incubated with MNBs were counted and digested with 250 μL of a concentrated H_2O_2/HNO_3 (1/2) solution for 3 h in a hot bath at 55 °C, under sonication (in order to ensure the complete digestion of the cells components). After this step, which lead to the complete evaporation of H2O2, concentrated HCl was added (3/1 volume ratio respect to HNO_3) to reach a final volume of 500 μL. The digestion proceeded overnight at room temperature. The solution was then diluted to 5 mL with milliQ water and filtered with a PVDF filter (0.45 um) before the analysis. The intracellular Fe concentration was measured by inductively coupled plasma atomic emission spectrometry (ICP-AES, Thermofisher ICAP 6300 duo) using a Fe calibration curve (linearity range between 0.01 - 10 ppm).

1.5 Reference

1. van Beijnum, J.R., et al., *Isolation of endothelial cells from fresh tissues.* Nat Protoc, 2008. 3(6): p. 1085-91.
2. Danila, D.C., M. Fleisher, and H.I. Scher, *Circulating Tumor Cells as Biomarkers in Prostate Cancer.* Clinical Cancer Research, 2011. **17**(12): p. 3903-3912.
3. Xu, H.Y., et al., *Antibody conjugated magnetic iron oxide nanoparticles for cancer cell separation in fresh whole blood.* Biomaterials, 2011. **32**(36): p. 9758-9765.
4. Myklatun, A., et al., *Microfluidic sorting of intrinsically magnetic cells under visual control.* Sci Rep, 2017. **7**(1): p. 6942.
5. Shahbazi-Gahrouei, D., et al., *Functionalized magnetic nanoparticles for the detection and quantitative analysis of cell surface antigen.* Biomed Res Int, 2013. **2013**: p. 349408.
6. Pan, Y., et al., *Magnetic nanoparticles for direct protein sorting inside live cells.* Chemical Science, 2012. **3**(12): p. 3495-3499.
7. Wang, E.C., L.K. Borysiewicz, and A.P. Weetman, *Cell Sorting Using Immunomagnetic Beads #*, in *T Immunochemical Protocols*. 1992. p. 347-357.
8. Tracey A. Martin, L.Y., Andrew J. Sanders, Jane Lane, Wen G. Jiang, *Cancer invasion and metastasis: molecular and cellular perspective*, in *Metastatic cancer: clinical and biological perspectives* L. Bioscience, Editor. 2013, Madame Curie Bioscience database.
9. Zhou, Y.L., et al., *Prognostic Value of Circulating Tumor Cells in Ovarian Cancer: A Meta-Analysis.* Plos One, 2015. **10**(6).
10. Krebs, M.G., et al., *Circulating tumour cells: their utility in cancer management and predicting outcomes.* Ther Adv Med Oncol, 2010. **2**(6): p. 351-65.
11. Thompson, J.C., et al., *Detection of Therapeutically Targetable Driver and Resistance Mutations in Lung Cancer Patients by Next-Generation Sequencing of Cell-Free Circulating Tumor DNA.* Clinical Cancer Research, 2016. **22**(23): p. 5772-5782.
12. Peled, N., et al., *A case series of ERBB2 indel driver mutations in non-small cell lung cancer identified by cell-free circulating tumor DNA NGS.* Cancer Research, 2016. **76**.
13. Nelmes, D.J., et al., *Detecting and monitoring somatic mutations in circulating cell free tumour DNA in patients with lung cancer.* Lung Cancer, 2016. **91**: p. S1-S1.
14. Mego, M., et al., *Correlation between blood markers of hemostasis and circulating tumor cells (CTCs) in early breast cancer patients.* Cancer Research, 2013. **73**.
15. Lopez-Munoz, E. and M. Mendez-Montes, *Markers of Circulating Breast Cancer Cells.* Advances in Clinical Chemistry, Vol 61, 2013. **61**: p. 175-224.
16. Croft, P., et al., *The science of clinical practice: disease diagnosis or patient prognosis? Evidence about "what is likely to happen" should shape clinical practice.* BMC Medicine, 2015. **13**.
17. Fan, Z., et al., *Theranostic nanomedicine for cancer detection and treatment.* Journal of Food and Drug Analysis, 2014. **22**(1): p. 3-17.
18. Society, A.C. *Survival rates for ovarian cancer, by stage*. Ovarian Cancer 2016 http://www.cancer.org/cancer/ovariancancer/detailedguide/ovarian-cancer-survival-rates].
19. Di Corato, R., et al., *Multifunctional nanobeads based on quantum dots and magnetic nanoparticles: synthesis and cancer cell targeting and sorting.* ACS Nano, 2011. **5**(2): p. 1109-21.
20. Materia, M.E., et al., *Mesoscale Assemblies of Iron Oxide Nanocubes as Heat Mediators and Image Contrast Agents.* Langmuir, 2015. **31**(2): p. 808-816.
21. Guardia, P., et al., *Water-Soluble Iron Oxide Nanocubes with High Values of Specific Absorption Rate for Cancer Cell*

Hyperthermia Treatment. Acs Nano, 2012. **6**(4): p. 3080-3091.
22. Guardia, P., et al., *One pot synthesis of monodisperse water soluble iron oxide nanocrystals with high values of the specific absorption rate.* Journal of Materials Chemistry B, 2014. **2**(28): p. 4426-4434.
23. Di Corato, R., et al., *Magnetic hyperthermia efficiency in the cellular environment for different nanoparticle designs.* Biomaterials, 2014. **35**(24): p. 6400-11.
24. Chen, C., et al., *Structural basis for molecular recognition of folic acid by folate receptors.* Nature, 2013. **500**(7463): p. 486-+.
25. O'Shannessy, D.J., et al., *Expression of folate receptors alpha and beta in normal and cancerous gynecologic tissues: correlation of expression of the beta isoform with macrophage markers.* Journal of Ovarian Research, 2015. **8**.
26. Stella, B., et al., *Design of folic acid-conjugated nanoparticles for drug targeting.* J Pharm Sci, 2000. **89**(11): p. 1452-64.
27. Teow, Y. and S. Valiyaveettil, *Active targeting of cancer cells using folic acid-conjugated platinum nanoparticles.* Nanoscale, 2010. **2**(12): p. 2607-2613.
28. Yang, H., et al., *Multifunctional Core/Shell Nanoparticles Cross-linked Polyetherimide-folic Acid as Efficient Notch-1 siRNA Carrier for Targeted Killing of Breast Cancer.* Scientific Reports, 2014. **4**.
29. Pearson, R.M., et al., *Tuning the Selectivity of Dendron Micelles Through Variations of the Poly(ethylene glycol) Corona.* Acs Nano, 2016. **10**(7): p. 6905-6914.
30. Yu, Y., et al., *Folate receptor-positive circulating tumor cells as a novel diagnostic biomarker in non-small cell lung cancer.* Transl Oncol, 2013. **6**(6): p. 697-702.
31. Liu, W.T., et al., *Folic acid conjugated magnetic iron oxide nanoparticles for nondestructive separation and detection of ovarian cancer cells from whole blood.* Biomaterials Science, 2016. **4**(1): p. 159-166.
32. Colombo, M., et al., *Protein oriented ligation on nanoparticles exploiting O6-alkylguanine-DNA transferase (SNAP) genetically encoded fusion.* Small, 2012. **8**(10): p. 1492-7.
33. Avvakumova, S., et al., *Development of U11-functionalized gold nanoparticles for selective targeting of urokinase plasminogen activator receptor-positive breast cancer cells.* Bioconjug Chem, 2014. **25**(8): p. 1381-6.
34. Galbiati, E., et al., *Peptide-nanoparticle ligation mediated by cutinase fusion for the development of cancer cell-targeted nanoconjugates.* Bioconjug Chem, 2015. **26**(4): p. 680-9.
35. Pelaz, B., et al., *Surface Functionalization of Nanoparticles with Polyethylene Glycol: Effects on Protein Adsorption and Cellular Uptake.* ACS Nano, 2015. **9**(7): p. 6996-7008.
36. Zhang, W.L., et al., *Gadolinium-Conjugated FA-PEG-PAMAM-COOH Nanoparticles as Potential Tumor-Targeted Circulation-Prolonged Macromolecular MRI Contrast Agents.* Journal of Applied Polymer Science, 2010. **118**(3): p. 1805-1814.
37. Lin, C.A.J., et al., *Design of an amphiphilic polymer for nanoparticle coating and functionalization.* Small, 2008. **4**(3): p. 334-341.
38. Hao, Y.Z., et al., *Impact of carbondiimide crosslinker used for magnetic carbon nanotube mediated GFP plasmid delivery.* Nanotechnology, 2011. **22**(28).
39. Dantola, M.L., et al., *Mechanism of photooxidation of folic acid sensitized by unconjugated pterins.* Photochem Photobiol Sci, 2010. **9**(12): p. 1604-12.
40. Hadjidemetriou, M. and K. Kostarelos, *NANOMEDICINE Evolution of the nanoparticle corona.* Nature Nanotechnology, 2017. **12**(4): p. 288-290.
41. Lesniak, A., et al., *Effects of the presence or absence of a protein corona on silica nanoparticle uptake and impact on cells.* ACS Nano, 2012. **6**(7): p. 5845-57.
42. Monopoli, M.P., et al., *Biomolecular coronas provide the biological identity of nanosized materials.* Nature Nanotechnology, 2012. **7**(12): p. 779-786.
43. Landgraf, L., et al., *A plasma protein corona enhances the biocompatibility of*

Au@Fe3O4 Janus particles. Biomaterials, 2015. **68**: p. 77-88.
44. Johnston, B.D., et al., *Colloidal Stability and Surface Chemistry Are Key Factors for the Composition of the Protein Corona of Inorganic Gold Nanoparticles.* Advanced Functional Materials, 2017. **27**(42): p. 1701956-n/a.
45. Lazzari, S., et al., *Colloidal stability of polymeric nanoparticles in biological fluids.* J Nanopart Res, 2012. **14**(6): p. 920.
46. Moore, T.L., et al., *Nanoparticle colloidal stability in cell culture media and impact on cellular interactions.* Chem Soc Rev, 2015. **44**(17): p. 6287-305.
47. Salvati, A., et al., *Transferrin-functionalized nanoparticles lose their targeting capabilities when a biomolecule corona adsorbs on the surface.* Nature Nanotechnology, 2013. **8**(2): p. 137-143.
48. Pablo Guardia, A.R., Simone Nitti, Giammarino Pugliese, Sergio Marras, Alessandro Genovese, Maria Elena Materia, Christophe Lefevre, Liberato Manna and Teresa Pellegrino, *One pot synthesis of monodisperse water soluble iron oxide nanocrystals with high values of the specific absorption rate.* J. Mater. Chem. B, 2014. **2**: p. 4426-4434.
49. Database, P.O.C. *Folic Acid*. 2017; Available from: https://pubchem.ncbi.nlm.nih.gov/compound/folic_acid#section=Top.